Institute of Space and Aeronautical Science, University of Tokyo
Report No. 518, November 1974

Kinetic Approach to the Evaporation and Condensation Problem

By

Masahide MURAKAMI* and Koichi OSHIMA

Summary: Phenomena caused in a vapor gas concerning evaporation from, or condensation onto a liquid (or solid) surface in contact with its pure vapor are investigated by using the Monte Carlo method. The formation of the Knudsen layer adjacent to the interphase and the growth of the hydrodynamic or continuum region outside the layer as time advances are simulated based on the kinetic theory of gases. The results are found to simulate these phenomena with sufficient accuracy. It is shown that there are two possible types of the transient developments of the vapor field according to the physical property of the evaporating substance. Several physical quantities in the hydrodynamic region in a quasi-steady state are computed and compared with a number of analytical and experimental data. The agreement of the present results with them is qualitatively satisfactory. A set of the slip condition at the interphase is presented to give the boundary conditions at the phase surface in hydrodynamic approaches. It is confirmed that the kinematic effects of binary collisions among vapor molecules on the mass flux rate are not so serious except in the case of very strong evaporation. This fact seems to indicate that the evaporation-condensation coefficient is close to unity provided that no condensation in the form of tiny droplets occurs in the vapor and that the mass accommodation (molecular absorption) coefficient of the phase surface is one. The quasi-steady state in the hydrodynamic region cannot be accomplished in both cases of the limiting condensation, where only condensation occurs but no molecules are spontaneously evaporated and reflected at the interphase, and of extremely strong evaporation, where the local Mach number in the continuum region exceeds unity. Some discussions on the feature of strong evaporation are also presented here.

I. INTRODUCTION

In the past several years, the study of evaporation from a liquid (or solid) surface or condensation onto it has been attained considerable importance in various fields of engineering as well as in physics and chemistry. Systematic researches for these phenomena are needed also in connection with astronautics to understand space-contamination phenomena of a vehicle and to estimate very small but often serious torque produced by evaporated vapor into vacuum from an adhesive joint or some other components of a vehicle. Since a heat pipe is a heat transfer device closely related to evaporation and condensation phenomena, such investigations also seems to provide with a good estimation of its performance.

* Post Graduate Fellow.
Present address; Ames Research Center, NASA, Moffet Field, CA. 94035, U.S.A.

Evaporation and condensation of gases are subject both to the kinematic behavior of gas molecules interacting with themselves and to the physical property of the condensed substance including the gas-surface interaction. The present study is concerned only with the former. In this field, a free molecular therory had been presented by Hertz [*1*] and Knudsen [*2*], which will be described as H-K theory hereafter. It was improved by Schrage [*3*] taking into account of not only the diffusion of gas molecules but their convective motion to give a quantitatively satisfactory result with respect to the flux rate except in the case of strong evaporation. However, the profile of the flow field accompanied with phase exchange is not predicted by these approaches. That is still derived based on the free molecular flow theory. The parameters appeared in this formula have to be obtained experimentally or by solving the Boltzmann equation. One of the main reasons why the Boltzmann equation should be solved is that a non-equilibrium layer, or the Knudsen layer, whose role can not be revealed at all by any hydrodynamic approaches, always exists adjacent to any phase boundaries. The equation has been treated to investigate these phenomena by several authors. The method of moments was employed by Kucherov and Rikenglaz [*4*], Patton and Springer [*5*] and Shankar and Marble [*6*] to give the mass flux rate, the heat flux rate and the slip conditions at the interphase. The linearized BGK equation has been solved analytically by Pao [*7*-a, b, c] and by Sone and Onishi [*8*] and numerically by Matsushita [*9*]. For the situation where the linearized BGK equation is valid, the flow field has been solved and the slip condition at the interphase has been exactly presented by the authors. Kogan and Makashev [*10*] obtained some numerical results solving the non-linear BGK equation and found that the flux rate was greater than that estimated by using the H-K theory by a factor 2 and more. Their computation covered fairly wide range of the magnitude of the evaporation rate. The ultimately strong evaporation, evaporation into vacuum, was investigated by the use of the method proposed by Mott-Smith for the Boltzmann equation [*11*, *12*] and using the matching expansion method by Edwards and Collins [*13*] for evaporation from a spherical source.

Many experimental studies have been made mainly for the purpose to get the evaporation or condensation coefficient, f, of various substances which is defined as the ratio of the actual evaporation or condensation rate to that estimated using Schrage's formula as given explicitly later. It follows from these experiments that the value of f is nearly equal to unity for several pure substances especially for many liquid or solid metals (for example 14, 15). This fact was found to be almost valid even in the case of ultimately strong evaporation of tantalum [*16*]. It has been emphasized that the value of f much smaller than unity was derived incorrectly from some experimental errors, from something like surface contamination and from the presence of noncondensable gases [*15*, *17*]. The same conclusions have been also reached theoretically by Huang [*18*]. It does not seem to be conclusive that the coefficient f is unity for every substance under any circumstanaces. Several factors affecting the coefficient, for example, the mass accom-

modation (molecular absorption) coefficient of the phase surface and the occurrence of homogeneous or heterogeneous condensation in the vapor, still are not wholly understood [*19*].

In this paper the Boltzmann equation governing these phenomena is solved by the use of the Monte Carlo method, where a kind of numercial experiment is conducted. The transient behavior in the vapor phase is followed numerically to examine a microscopic structure of a evaporating or condensing system and the role of the non-equilibrium Knudsen layer. Several hydrodynamic quantities in the vapor phase, the flux rate and the value of f under a quasi-steady condition are computed and compared with a number of available data. A set of macroscopic slips is presented to be applied as the exact boundary conditions in hydrodynamic approaches. Effects of the molecular absorption coefficient of the phase surface on the phenomena are examined. The feature of strong evaporation is pursued both qualitatively and quantitatively. The limiting case of the quasi-steady evaporation and the maximum value of the evaporation rate are found as a result.

II. Transient Evaporation and Condensation Problem

The following one-dimensional and time-dependent problem is considered here: Initially, a liquid (or solid) is in equilibrium with its pure vapor occupying the the half-space ($x \geqslant 0$) at the temperature T_0 and the pressure P_0 as shown in Fig. 1, where the direction for use of subscripts, 0, ∞, 1 and L, is also given. At an instant $t=0$, the surface temperature of the condensed phase discontinuously changes to T_L and is kept at this value throughout the procedure. Then, evaporation or condensation begins through the phase surface according to a relation among T_0, P_0, T_L and P_L which is the saturation vapor pressure of the condensed material at the temperature T_L. It is the behavior of the vapor occupying the half-space that will be pursued here. Thus, some other phenomena possibly caused in the condensed phase, for example, heat conduction and boiling in the liquid, are left out of consideration. This means that only surface evaporation is treated in the case of evaporation while for condensation more general situations are studied. It is also left out of account the formation of the clusters and the droplet-wise

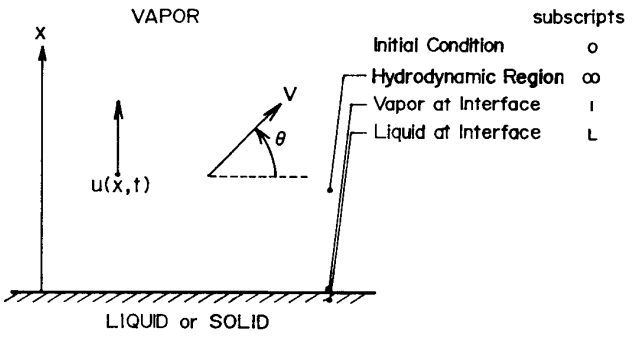

FIG. 1. Configuration for problem and direction for use of the subscripts.

condensation in the vapor phase. It appears that these phenomena become sometimes important in evaporation-condensation phenomena. The possibility of their occurrences even in a pure vapor will be also pointed out in the latter part of this paper. Such a surface evaporation could be caused under several circumstances, e.g., when a system is in nearly equilibrium or when a liquid (or solid) surface is exposed to laser radiation [*11*]. However, it is justifiable to consider that the displacement of the phase surface due to evaporation or condensation negligibly small. The vapor is supposed to behave as an ideal monatomic gas and to condense only on the interphase. It is also assumed that the gas molecules evaporated spontaneously from the interphase have a Maxwellian distribution corresponding to T_L and P_L, and that the number flux rate τ_L is given by the usual formula

$$\tau_L=\alpha P_L/\sqrt{2\pi mkT_L} \tag{1}$$

with the aid of the absorption coefficient α, where m and k are the molecular mass and the Boltzmann constant, respectively. An α part of the molecules incident on the interphase is absorbed there (condensation) and the rest is re-emitted (re-evaporation) diffusely according to an equilibrium distribution corresponding to T_L and P_L. This implies that the re-emitted molecules completely accommodate. The value of α is usually obtained experimentally [*17*].

The state of the vapor field is time-dependent as a whole, because the evaporation or condensation wave front is always traveling into the gas region. Nevertheless, a quasi-steady state is, in general, accomplished firstly in the neighborhood of the interphase in a rather short time, which is still sufficiently large compared with a mean free time of the gas, after the evaporation or condensation front passes over. The region in this state, which will be referred to as the uniform region, extendes into the gas as time advances. Therefore, every computation should be continued until a quasi-steady condition is attained in the hydrodynamic, or continuum region.

III. Monte Carlo Method

The Monte Carlo method employed in the present investigation is similar to the direct simulation method proposed by Bird [*20*]. The vapor molecules are assumed to interact on each other obeying an inverse power law of repulsion of $F=ar^{-5}$, where r is the distance between the molecules, that is, they behave as the Maxwellian molecules. This assumption enables one to make the formulation considerably simple and to shorten the time required for the computation. Besides, it is supposed that the absorption coefficient α is a constant to be assigned. It is natural that the molecular chaos is assumed to be valid among the vapor molecules. The present method of simulation is constructed based on the following two facts. The first is that the molecular collisions can be approximately separated from their translational motions during a time interval Δt provided that Δt is sufficiently smaller than the mean free time of the gas. The other is that, when the vapor

field is subdivided into N layers (cells) parallel to the phase surface with each width of Δx, the state of the vapor may be regarded as almost spatially uniform in every cell and the differences of the physical quantities of the adjoining two cells are very small if Δx is much smaller than the mean free path of the vapor in any condition. In addition to these conditions, Δt and x have to be much smaller than any characteristic scales of their own dimensions in this system throughout the procedure to conduct the simulation.

The general procedure of the simulation is shown in a computer flow chart (Fig. 2). The initial condition of the vapor, T_0 and P_0, and the state of the liquid (or solid) surface, T_L and P_L, are specified as a set of the input data arranged in the forms of n_0/n_L and a parameter β defined by

$$\beta=[(n_L-n_0)/n_0]/[(T_L-T_0)/T_0], \tag{2}$$

where n represents the number density. It is easy to see that β directly relates to the derivative of the number density at the evaporating surface with respect to the temperature. The values of Δx and Δt are in fact decided so that they are as large as possible to shorten the computational time but small enough to satisfy the required conditions. Thus, every quantity is evaluated as its average value in each cell during an interval Δt. The test particles are distributed in the vapor field according to a Maxwellian distribution corresponding to T_0 and P_0. In the present computation, they are only allocated equally among the cells by N_0 because of the

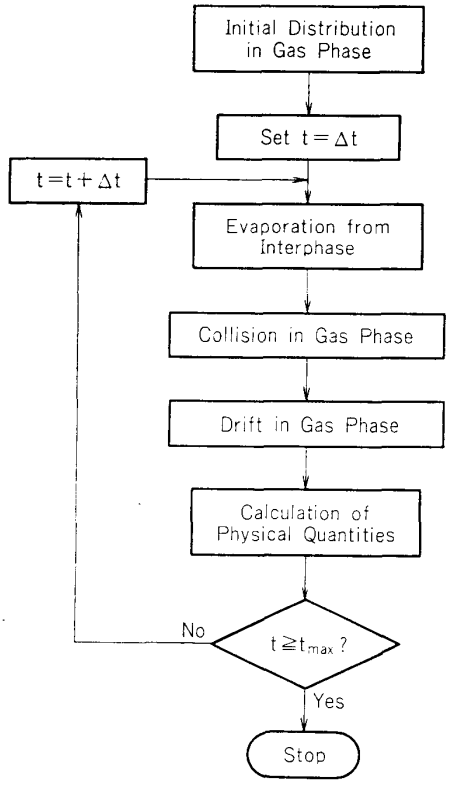

FIG. 2. Computer flow chart of simulation.

assumption of the uniformity of state in each cell. The upper limit of the computational field is extended as time advances, which assures that the state of the undisturbed vapor retains at the initial stage. Thus, the preliminary arrangements for the simulation are completed. The spontaneous evaporation from the phase surface is made according to a Maxwellian distribution corresponding to T_L and P_L with zero mass velocity independently of the state of the gas phase. The evaporated particles proceed in the vapor field with their assigned velocities during Δt. Then, the molecular collisions are simulated during Δt in all the cells to give the new molecular velocities of some test particles after collision. At the next stage, each particle drifts to a new location with its own velocity. The particles incident on the phase surface are either absorbed to condense or reflected diffusely (re-evaporation). A series of procedures, i.e., the spontanaeous evaporation, the collision and the drift, are repeated during the desired duration. Hydrodynamic quantities in the vapor phase except the number density which is calculated in every cycle of the procedure because it is required to evaluate the collision frequency are computed from the velocity distribution of the test particles if necessary. The number flux rate at the interphase is calculated in terms of the particle number absorbed and reflected there. An examination whether the requirements for Δt and Δt are satisfied is occasionally made.

Three values, x, V and θ, as shown in Fig. 1, are stored per each test particle using each 255 distrete values for the sake of the finite computer capacity. Thus, only the number of the cell to which a test particle belongs is stored instead of its spatial coordiante x because the validity of the spatially uniform distribution of the particles in each cell is assured. For the polar angle θ, the whole angle over $-\pi/2$ to $\pi/2$ is equally divided into 255 discrete values. The interval of the quantity $V/\sqrt{2RT_0}$ from 0 to 6.24 is suitably subdivided into 255 pieces according to the specified condition of T_0 and T_L. Since only 24 bits of the core memory are needed to store the character of a test particle, such a scheme enable us to employ nearly 35000 particles using a computer with 65 KW core memory.

Random numbers obeying several statistical distributions are drawn with the aid of pseudo-random numbers uniformly distributed on (0,1), whose generators consist of the shift and the add statements for a high speed digital computer. They were previously examined with respect to the average value, the standard deviation, the periodicity and so on.

3.1. Reference Quantities

This system possesses two characteristic dimensions, the mean free path and the mean free time of the vapor, from the microscopic point of view, but there are no such in the macroscopic framework. The mean free path of the vapor at the initial stage, λ_0, is taken as the referance length of this system, defined by the following formula

$$\lambda_0=\frac{1}{3\sqrt{\pi}A_2(5)n_0}\left(\frac{kT_0}{a}\right)^{1/2} \qquad (3)$$

for the Maxwellian molecules, where $A_2(5)$ is obtained from the scattering integral as

$$A_2(5)=\int_0^\infty \sin^2\chi\tilde{b}d\tilde{b}=0.436. \tag{4}$$

Here, χ and $\tilde{b}$ are the deflection angle and the dimensionless impact parameter, respectively, as explicitly given later. A quantity t_0 defined by

$$t_0=\frac{\lambda_0}{C_{m0}}.$$

where C_{m0} is the most probable speed of the vapor at initial stage and equals $\sqrt{2RT_0}$, is employed as the reference time. It is clear that this quantity is of the order of the mean free time of the vapor at the initial stage. For convenience's sake, all quantities are treated in the corresponding dimensionless forms with regard to the above two and the quantities at the initial stage, n_0, C_{m0}, T_0, P_0 and q_0, where q_0 is the heat flux in the x-direction. The values of Δx and Δt must be specified so that they satisfy at least the condition that $\Delta x \ll \lambda_0$ and $\Delta t \ll t_0$, respectively.

3.2. Initial Distribution in the Gas Phase

The particle number N_0 to be allocated to a cell is decided so that the values of u and T evaluated from the N_0 test particles become approximately equal to zero and T_0, respectviely, with reasonable accuracy. The distribution of the test particles in the velocity space is generated from a Maxwellian one with zero mass velocity as

$$f_0(V)=n_0\left(\frac{1}{\sqrt{\pi}C_{m0}}\right)^3\exp\left(-\frac{V^2}{C_{m0}^2}\right). \tag{5}$$

where V is the magnitude of the molecular velocity $\bar{V}$. The probability of the particles in the velocity range $(V, V+dV)$ is expressed as

$$\frac{f_0(V)}{n_0}d\bar{V}.$$

Thus, the particle obeying the desired distribution is picked from the cumulative function, f_G, as

$$F_g=\int_0^{\bar{V}}\frac{f_0(V')}{n_0}d\bar{V}', \tag{6}$$

where the primes indicate the dummy variables. This is transformed using the spherical polar coordinate system as shown in Fig. 3 to result in

$$F_G=\int_0^{\phi}\frac{d\phi'}{2\pi}\int_{-\pi/2}^{\theta}\frac{\cos\theta'}{2}d\theta'\int_0^V\frac{4}{\sqrt{\pi}C_{m0}^3}V'^2\exp\left(-\frac{V'^2}{C_{m0}^2}\right)dV', \tag{7}$$

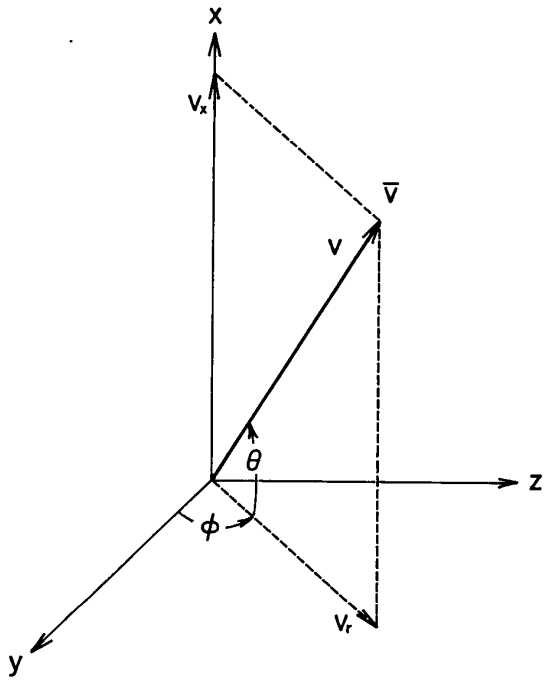

FIG. 3. Coordinate system.

where ϕ and θ are the azimuth angle and the polar angle, and the following relations are used.

$$V_x = V \sin\theta$$
$$V_y = V \cos\theta \cos\phi$$
$$V_z = V \cos\theta \sin\phi.$$

It follows from the equation (7) that three events with respect to ϕ, θ and V happen independently. Then, the required random variables, ϕ, θ and V, are obtained using three pseudo-random numbers, R_ϕ, R_θ and R_V uniformly distributed on (0, 1) as follows.

$$\left.\begin{aligned} &\frac{\phi}{2\pi} = R_\phi \\ &\frac{\sin\theta}{2} + 1/2 = R_\theta \\ &\operatorname{erf}\left(\frac{V}{C_{m0}}\right) - \frac{2}{\sqrt{\pi}} \frac{V}{C_{m0}} \exp\left(-\frac{V^2}{C_{m0}^2}\right) = R_V. \end{aligned}\right\} \tag{8}$$

In fact, the value of ϕ need not be picked in this problem because of the geometry.

3.3. Spontaneous Evaporation

The true number of molecules evaporated spontaneously per unit area during Δt is $\tau_L \Delta t$, where τ_L is defined in the equation (1). Thus, the particle number emitted from the interphase is $[N_0 \tau_L / n_0](\Delta t / \Delta x)$ in this computation. The probability density function of the emitted molecules is $[V_x f_L(V)/\tau_L]$. The cumulative distri-

bution function, F_E, is given using the cylindrical coordinate system as shown in Fig. 3 by

$$F_E=\int_0^{\bar{V}}\frac{V'_x f_L(V')}{\tau_L}d\bar{V}'=\int_0^{\phi}\frac{d\phi'}{2\pi}\int_0^{V_x}\frac{2V'_x}{C_{mL}^2}\exp\left(-\frac{V'^2_x}{C_{mL}^2}\right)dV'_x \int_0^{V_r}\frac{2V'_r}{C_{mL}^2}\exp\left(-\frac{V'^2_r}{C_{mL}^2}\right)dV'_r \tag{9}$$

Noting the following relation

$$\int_0^{V_x}\frac{2V'_x}{C_{mL}^2}\exp\left(-\frac{V'^2_x}{C_{mL}^2}\right)dV'_x=-\exp\left(-\frac{V_x^2}{C_{mL}^2}\right)+1, \tag{10}$$

V is derived using two random numbers, R_x and R_r, from

$$V^2=-C_{mL}^2\ln(R_xR_r), \tag{11}$$

as presented in the reference 21. Another expression of F_E in the spherical polar coordinate system as

$$F_E=\int_{-\pi/2}^{\theta}2\sin\theta'\cos\theta'd\theta'\int_0^{\phi}\frac{d\phi'}{2\pi}\int_0^{V}\frac{2V'^3}{C_{mL}^4}\exp\left(-\frac{V'^2}{C_{mL}^2}\right)dV'$$

suggests that the variable θ is easily computed from the relation as

$$\sin^2\theta=R_\theta. \tag{12}$$

The velocity of each evaporated molecule is assigned in this way, and it goes forward from the interphase to a location, $\bar{V}\cdot\Delta t$, without collisions during Δt. It is another important criterion in order to simulate precisely the gas behavior in the vicinity of the interphase that the values of Δx and Δt must be specified so that almost all of the newly evaporated particles fall in the cell adjacent to the interphase. After completion of the evaporation process, the number density of each cell is calculated provisionally for the sake of further convenience. This value is used only in the next stage provisionally.

3.4. Collision Process

A pair of particles to collide may be chosen among the particles in a cell independently of their relative location owing to the condition posed on the magnitudes of Δx and Δt. The collision probability is proportional to $g^{(\nu-5)/(\nu-1)}$, where g is the maghitude of the relative velocity $\bar{g}$ and ν is the exponent in the force law. It is obvious that the probability becomes independent of g in the case of $\nu=5$, say, Maxwellian molecules. Thus, every collision pair in a cell is found in equal probability. The time increment per a collision in the i-th cell, Δt_{ci}, is

$$\Delta t_{ci}=\frac{2}{N_i}\left[\pi\tilde{b}_m^2\left(\frac{2a}{m}\right)^{1/2}n_i\right]^{-1}, \tag{13}$$

where N_i and n_i are the particle number and the number density of the i-th cell, respectively, and $\tilde{b}_m$ is the cut-off value of the dimensionless impact parameter taken to be 1.5 as in several previous works. For convenience, the impact parameter b is treated in such a dimensionless form $\tilde{b}$ as

$$\tilde{b}=b\left(\frac{mg^2}{2a}\right)^{1/4} \tag{14}$$

The collision plane is fixed using a parameter ε, which is defined as an angle between a unit vector $\bar{n}$ in the plane of collision and an arbitrary plane measured in a plane perpendicular to $\bar{g}$. Thus,

$$\cos\varepsilon=\bar{n}\cdot\bar{a}, \tag{16}$$

where $\bar{a}$ is a unit vector in the arbitrary plane.

The arbitrary plane is conveniently chosen so as to be normal to the x-axis. The probability that the collision parameters fall between $\tilde{b}$, $\tilde{b}+d\tilde{b}$ and ε, $\varepsilon+d\varepsilon$, as illustrated in Fig. 4, is

$$\tilde{b}d\varepsilon d\tilde{b})/\pi\tilde{b}_m^2.$$

The values $\tilde{b}$ and ε are computed from two random numbers R_b and R_ε, respectively, as follows,

$$\left.\begin{aligned}\tilde{b}&=\tilde{b}_m\sqrt{R_b}\\ \varepsilon&=2\pi R_\varepsilon.\end{aligned}\right\} \tag{17}$$

Thus, all the parameters needed to decide a collision are settled together with the velocities of the colliding particles stored.

The deflection angle χ is written with the aid of the angle of the apse line ϕ as

$$\chi=\pi-2\phi. \tag{18}$$

Here, ϕ is evaluated from an integral as

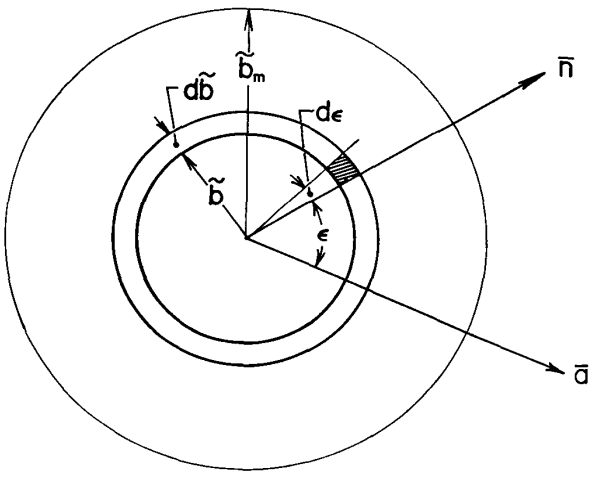

FIG. 4. Illustration of $\tilde{b}$ and ε.

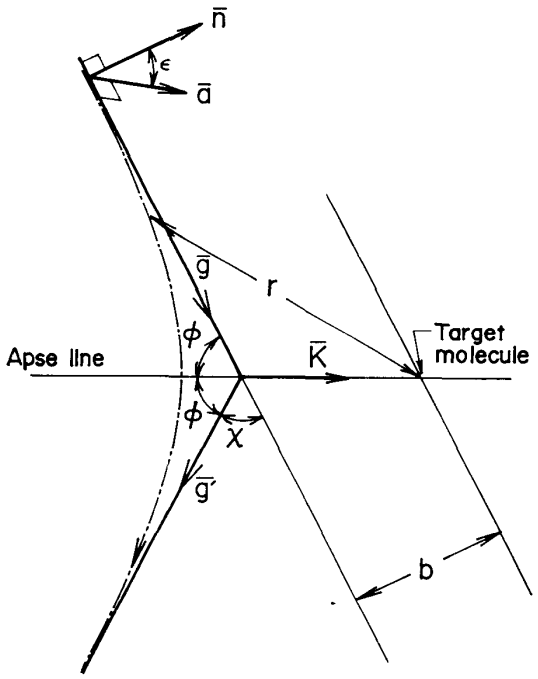

FIG. 5. Collision plane.

$$\phi=\int_{r_{00}}^{\infty}\left(\frac{r^4}{b^2}-r^2-\frac{4r^4\Psi(r)}{mb^2g^2}\right)^{-1/2}dr \tag{19}$$

for the field with the intermolecular potential $\Psi(r)$, which is assumed to be symmetric, as shown in Fig. 5. Here, r is the distance between the molecules and r_{00} is a root of the equation

$$\frac{r^4}{b^2}-r^2-\frac{4r^4}{mb^2g^2}\Psi(r)=0. \tag{20}$$

For the case of Maxwellian molecules, it results in

$$\phi=\int_{r_{00}}^{\infty}\left(\frac{r^4}{b^2}-r^2-\frac{a}{mb^2g^2}\right)^{-1/2}dr. \tag{21}$$

It is shown in the reference 22 that this may be rewritten in terms of the elliptic integral of the first kind $K\{k^2\}$ after performing a suitable transformation as follows

$$\phi=\left(1+\frac{2}{\tilde{b}^4}\right)^{-1/4}K\left\{\frac{1}{2}\left[1-\left(1+\frac{2}{\tilde{b}^4}\right)^{-1/2}\right]\right\},$$

where

$$K\{k^2\}=\int_0^{2\pi}(1-k^2\sin^2\theta')^{-1/2}d\theta'.$$

The velocity after collision is expressed with the aid of the velocity before collision and the angle ϕ. Supposing a collision between the i-th particle and the k-th

one, the classical mechanics shows the following relations among their velocities $\bar{V}_i, \bar{V}_k, \bar{V}'_i$ and $\bar{V}'_k$ as

$$\left.\begin{aligned}&(\bar{V}_k-\bar{V}_i)-(\bar{V}'_k-\bar{V}'_i)=2g\cos\phi\bar{K}\\&\bar{V}_k+\bar{V}_i=\bar{V}'_k+\bar{V}'_i\\&g=g',\end{aligned}\right\} \tag{22}$$

where the primes denote the quantities after collision, and $\bar{K}$ is a unit vector on the apse line as given in Fig. 5. Then it follows from the equation (22) that

$$\left.\begin{aligned}&\bar{V}'_k=\bar{V}_k-g\cos\phi\bar{K}\\&\bar{V}'_i=\bar{V}_i+g\cos\phi\bar{K}.\end{aligned}\right\} \tag{23}$$

The vector $\bar{K}$ is expressed in terms of the vectors $\bar{n}$ and $\bar{g}$ as

$$\bar{K}=\bar{n}\sin\phi+\bar{g}\cos\phi/g.$$

The unit vector $\bar{n}$ normal to $\bar{g}$ in the plane of collision is obtained from the following relations among $\bar{n}, \bar{a}$ and $\bar{g}$ as

$$\left.\begin{aligned}&|\bar{n}|^2=1\\&\bar{a}\cdot\bar{n}=\cos\varepsilon\\&\bar{n}\cdot\bar{g}=0.\end{aligned}\right\} \tag{25}$$

The results are

$$\left.\begin{aligned}n_x&=-\frac{(g_y^2+g_z^2)^{1/2}\sin\varepsilon}{g}\\n_y&=\frac{g_xg_y\sin\varepsilon-gg_z\cos\varepsilon}{g(g_y^2+g_z^2)^{1/2}}\\n_z&=\frac{g_xg_z\sin\varepsilon+gg_y\cos\varepsilon}{g(g_y^2+g_z^2)^{1/2}}.\end{aligned}\right\} \tag{26}$$

Thus, new velocities of the molecules after a collision are computed in terms of $\bar{n}$. These procedure is repeated till the total time spent for collisions, $\Sigma\Delta t_{ci}$, exceeds the interval Δt in each i-th cell.

3.5. Drift Process

Each particle moves from a point $\bar{x}_0$ to a new location $\bar{x}_0+\bar{V}\cdot\Delta t$ during Δt, where $\bar{x}_0$ and $\bar{V}$ are the space and the molecular velocity vectors, respectively. Since the spatial distribution of particles in a cell is assumed to be uniform, the point, say $\bar{x}_0$, is assigned randomly in the range over $(i-1)\Delta x$ to $i\Delta x$ in the i-th cell. Some of the particles are incident on the phase surface or on the upper limit of the computational field, while the rest remain in the gas phase. Those incident on the computational boundary are reflected specularly there and those on the interphase are absorbed there to condense or reflected diffusely. The number of absorbed particles

on the interphase, NA, and that of reflected ones, NR, are stored to compute the number flux rate at the interphase.

After the aforementioned processes from 3.3 to 3.5 are completed, the time is advanced by Δt and some desired quantities are calculated, if necessary.

3.5. Hydrodynamic Quantities

A mean value of φ, $\langle\varphi(\bar{x}, t)\rangle$, is determined with the aid of the Boltzmann function f as

$$\langle\varphi(\bar{x}, t)\rangle=\frac{1}{n}\int\varphi f d\bar{V}, \tag{27}$$

which is nothing but a definition of a hydrodynamic quantity. Thus, the hydrodynamic quantities in the i-th cell is analogously obtained from the distributions of N_i test particles by

$$\langle\varphi_i(t)\rangle=\frac{1}{N_i}\sum_{j=1}^{N_i}\varphi_j. \tag{28}$$

i) Number Density

$$n_i=\frac{N_i}{N_0}n_0 \tag{29}$$

ii) Mass Velocity in the x-direction

$$u_i=\frac{1}{N_i}\sum_{j}^{N_i}(V\sin\theta)_j=\frac{1}{N_i}\sum_{j}^{N_i}V_{xj}, \tag{30}$$

iii) Temperature

$$T_i=\frac{1}{3RN_i}\left[\sum_{j}^{N_i}V_j^2-N_iu_i^2\right] \tag{31}$$

iv) Pressure

$$P_i=kn_iT_i \tag{32}$$

v) Heat Flux in the x-direction

$$q_i=\frac{mn_i}{2}\frac{1}{N_i}\sum_{j}^{N_i}[(V_j^2+u_i^2-2u_iV_{xj})(V_{xj}-u_i)] \tag{33}$$

vi) Number Flux Rate

$$\tau_1=\tau_L-\frac{(NA-NR)}{\Delta t}\frac{n_0\Delta x}{N_0}\quad\text{(at the interphase)} \tag{34}$$

$$\tau_i=u_in_i. \tag{35}$$

It is natural that τ_1 becomes equal to τ_i $(i=2, 3, \cdots, N)$ after a quasi-steady state will be accomplished.

IV. Results and Discussions

In the course of the present investigation, the computational condition is specified with the aid of α, β and n_0/n_L. In the case where n_0/n_L is less than unity, evaporation, generally, (but not always) occurs. The values of $\Delta x/\lambda_0$ and $\Delta t/t_0$ are prescribed depending on the computational condition and are kept less than 0.2 and 0.02, respectively, in any cases.

A typical computational result in the early stage of evaporation is shown in Fig. 6. Some parameters, for example, Δx, Δt and N_0 etc., are decided so that the computational error should not exceed several per cent of each quantity but the computational time should be reasonable. In some cases where such an accuracy cannot be attained or where more accurate results are desired, a spatially-and/or time-averaged value are also employed as a quasi-steady value in the hydrodynamic region.

A transient development of the vapor phase in the case of strong evaporation is given in Fig. 7, where the numerical results are smoothed at three locations. Here $(nu)_1$ stands for the flux rate at the interphase evaluated by the use of the equation (34) and then time-averaged over several times of Δt around each instant. It is easy to see that a quasi-steady state is possibly accomplished after the evapo-

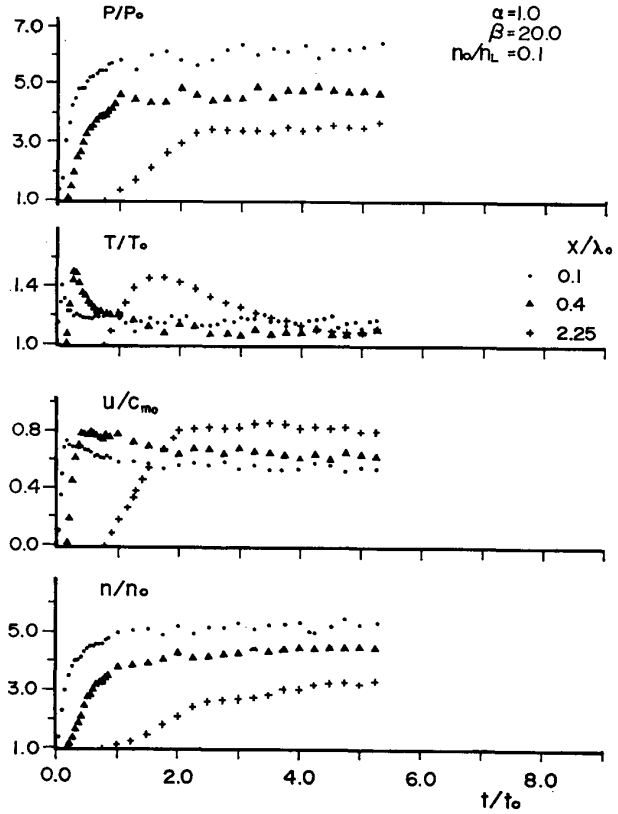

Fig. 6. Transient development of gas phase in early stage.

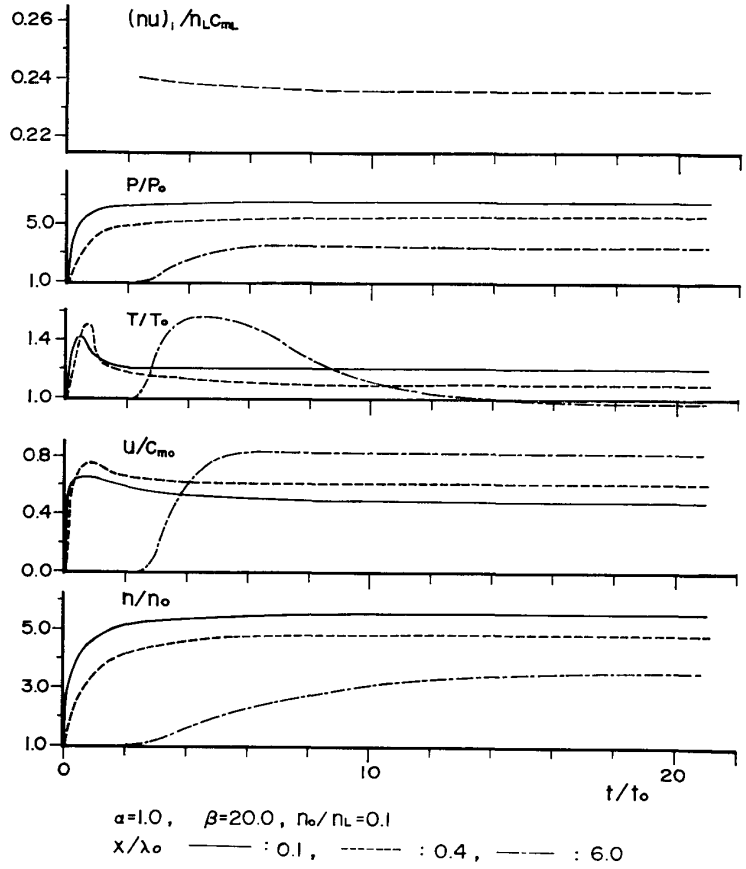

FIG. 7. Transient development of gas phase (smoothed)

ration wave passing over in this case. The time interval required for the accomplishment which is larger than ten times of t_0 increases with the distance from the interphase because of the diffusion of the evaporation wave front as its propagation. However, in the case of very strong evaporation, where the traveling evaporation wave turns into a shock wave, such a quasi-steady state is not expected to be attained outside the Knudsen layer. A number of preliminary examinations including this suggest that it causes no trouble to limit the computational field within $x=50\,\lambda_0$ and the duration up to $40t_0$ in order to compute the quasi-steady quantities in the hydrodynamic region.

The profiles of several physical quantities in the vapor field are illustrated for three computational conditions in Figs. 8-a, b, c. In these figures, some computed points are omitted for brevity. The former two show those in the case of strong evaporation for $\alpha=1.0$, $\beta=20.0$ and $n_0/n_L=0.1$, and for $\alpha=1.0$, $\beta=1.0$ and $n_0/n_L=0.3$, respectively, while the last is for condensation. In the early stage within an interval of a few times of t_0, the initial discontinuity at the interphase rapidly distorted and it turns into a traveling wave of compression-type as in the case given in Fig. 8-a or only becomes smooth more and more as in Fig. 8-b. Thus, the initial layer (Ref. 23) is accomplished, which cannot be presented by any hydrodynamic approaches. While from the spatial point of view, the Knudsen layer where the vapor molecules are in non-equilibrium state is formed adjacent

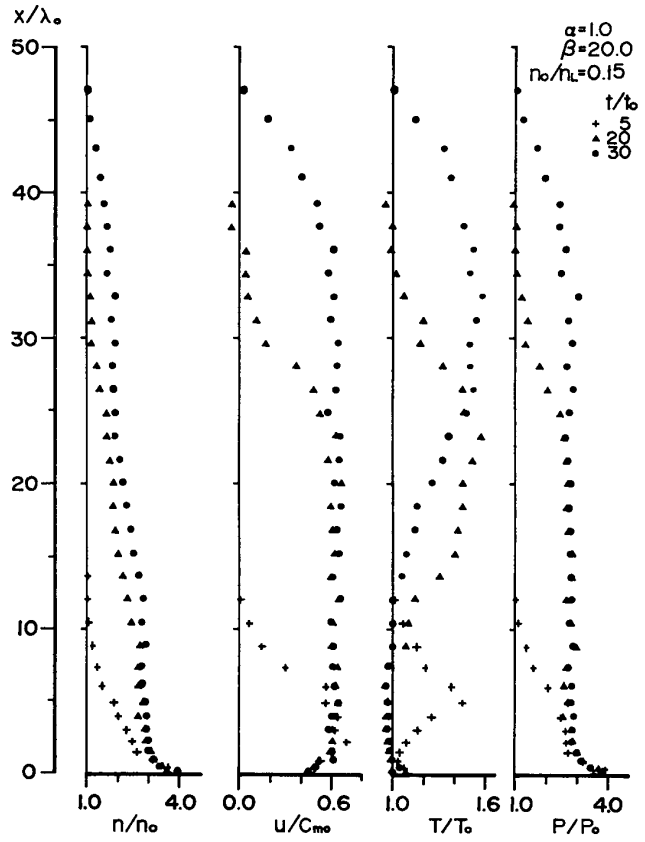

FIG. 8. (a)

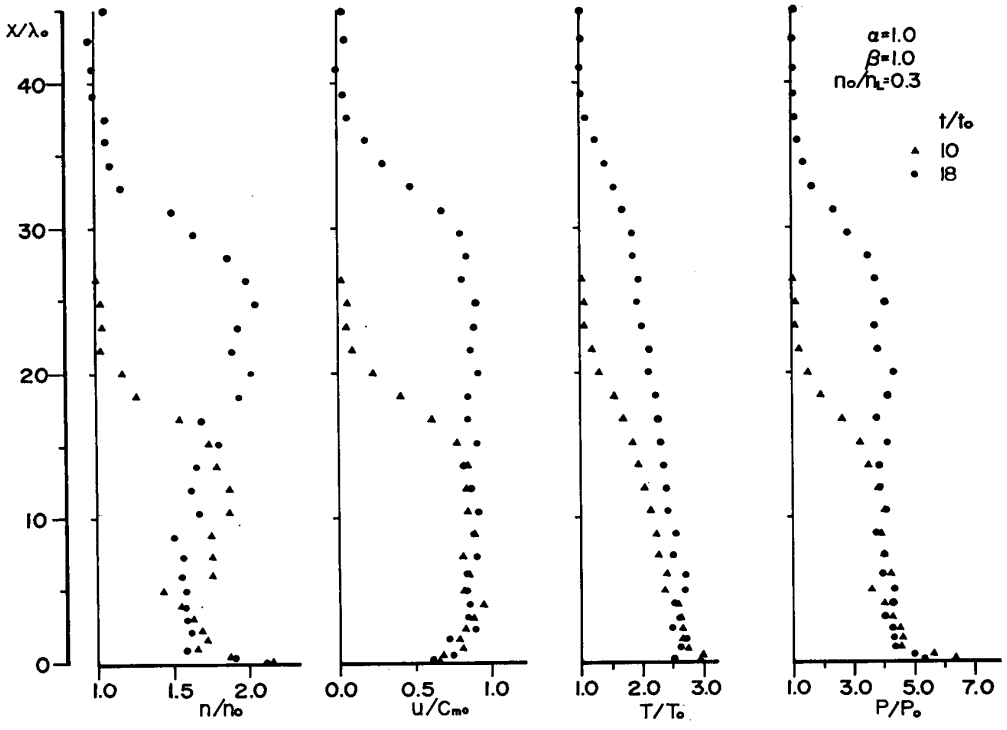

FIG. 8. (b)

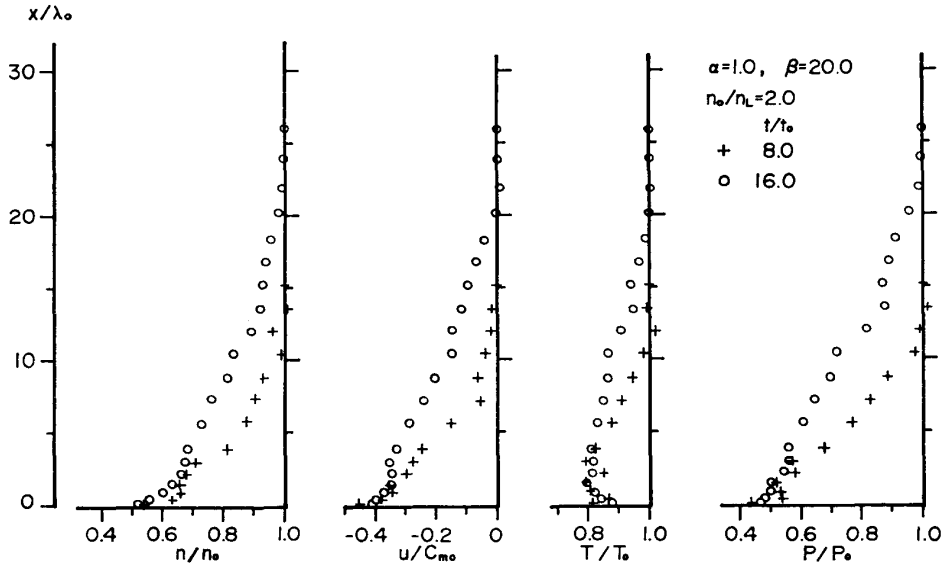

FIG. 8. (c)

FIG. 8-a,b,c. Vapor field profiles.

to the phase surface as shown in detail in Figs. 9-a, b also. After the completion of the non-equilibrium Knudsen layer with the thickness of several mean free paths, the evaporation front travels into the vapor diffusing its front and a quasi-steady region grows outside the layer in the hydrodynamic region behind the front. Such a quasi-steady state cannot be accomplished in the case of the limiting condition, where only condensation occurs but no molecules are spontaneously evaporated and reflected at the interphase, and extremely strong evaporation, where the evaporation front turns into a shock wave and the rarefaction wave propagates into the hydrodynamic region outside the Knudsen layer after the completion of the layer. It is quite natural that the behavior of the vapor in the neighborhood of the condensation wave in the strong case can be satisfactorily approximated by that of a traveling rarefaction wave if the traveling speed is specified by the use of the present result. Every physical quantity of the vapor at $x=0$ in general differs from that of the liquid (or solid) surface and such a discrepancy is termed as the microscopic slip. In the Knudsen layer, every variation of the hydrodynamic quantity is very steep and is of the order of the magnitude itself measured in the hydrodynamic region. Such a situation resembles that of a surface shock wave, or to be more exact, a surface strong rarefaction wave. Both the microscopic slip and the variation in the Knudsen layer are considered as its discontinuity at a phase boundary in hydrodynamic approaches. This is nothing but the (macroscopic) slip which should be specified there as a boundary condition in such treatments. The state in the hydrodynamic region is found to depend strongly on all the parameters in the non-equilibrium layer especially in the case of strong evaporation, which is turn must be given only by solving the Boltzmann equation. Thus, the temporal and spatial development of this system consists of two phenomena caused in both the microscopic and the macroscopic scales. Those in the initial layer and in the Knudsen layer belongs to the former, while those in the hydro-

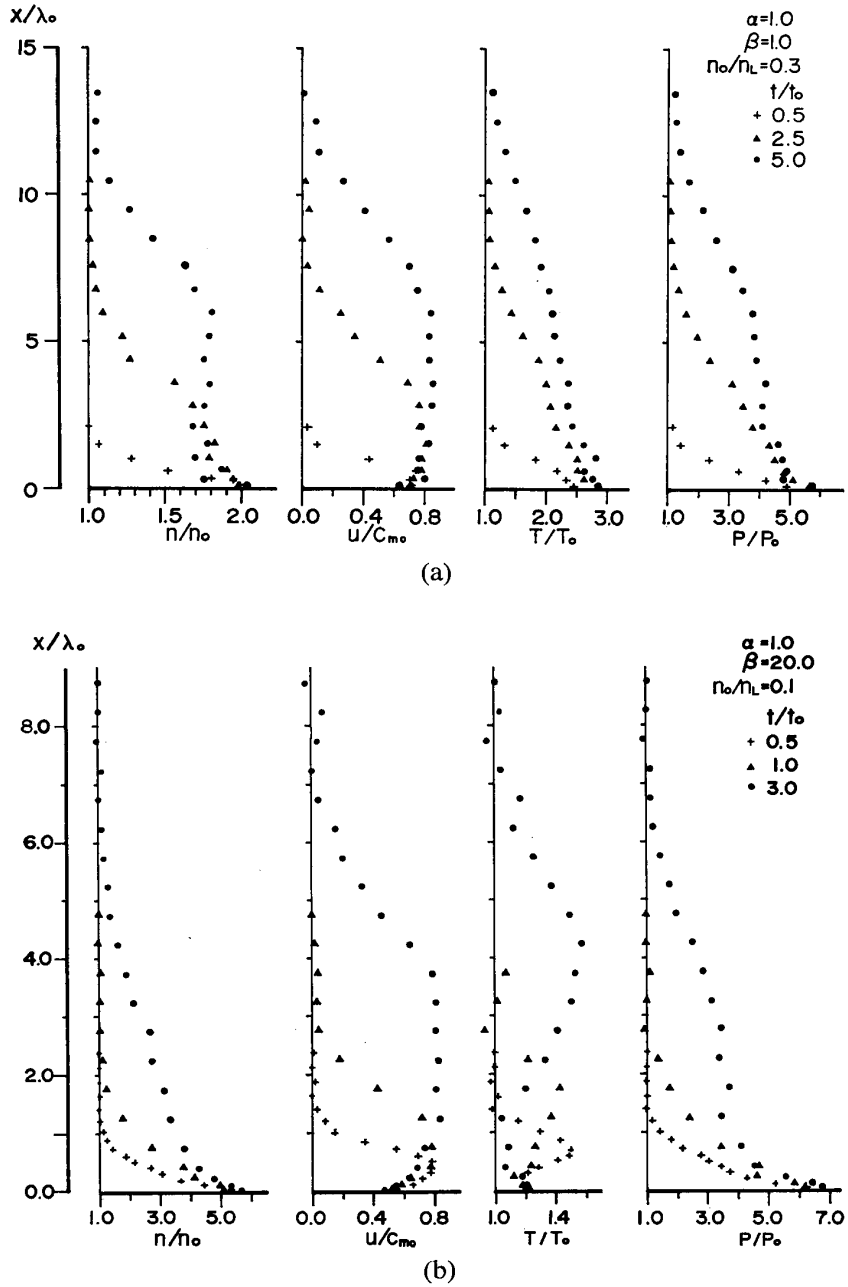

FIG. 9–a, b. Vapor field profiles in early stage.

dynamic region do to the latter, which can be described using the hydrodynamic equations. It becomes evident that two types of transient profiles are possible of realization depending on the value of β in the case of evaporation. In one case as shown in Fig. 8-a, the temperature rises at the evaporation wave front and falls gradually throughout the transition region in the hydrodynamic region to its quasi-steady value in the uniform region, while the number density increases considerably both at the front and at the boundary between the transient region and the uniform one and approaches to its quasi-steady value monotonously. In another case as in Fig. 8-b, the number density reaches the maximum value immediately behind the front but the temperature rises monotonously and reaches its quasi-steady value

in the asymptotic sense as time advances. The pressure and the mass velocity are, of course, uniform throughout the transition and the uniform regions in both cases. Thus, overshoots of the temperature and of the density take place in the former and the latter cases, respectively. It is evident that the feature of the former resembles that of a plane traveling compression wave though the evaporation wave is not a shock in this case. That is because for large value of β the evaporated vapor possesses the larger number density but the not-so-higher temperature than those of the vaper at initial stage and compresses the undisturbed vapor at rest. On the other hand, the latter is characterized by the higher temperature and the not-so-larger number density. Thus, the behavior shows that the feature due to energy transfer is comparable to or even dominant over the wave character for small β. However, when the evaporation wave turns to a shock wave for small value of n_0/n , the former profiles are realized even in the case of small value of β. It can be concluded that the transport phenomena in the vapor phase are caused by both the mass and the energy transportations and that the former takes place mainly in the form of a traveling compression wave and the latter does in a diffusion-like manner. It seems that the temperature profile for $\beta=20.0$ corresponds to that with negative gradient reported by Pao [7-a] concerning the two-surface steady problem. It is found that such transition between the two profiles occurs at a value of $\beta\simeq 3.6$ almost independently of the other parameters, provided that a shock wave is not formed, which is very close to the value of 3.5 presented by Pao [7-a] with respect to the occurrence of the negative temperature gradient. Though such a distinction between the profiles is not seen in the case of condensation, the temperature inversion is found to happen in the case of large value of β as given in Fig. 10-c. The parameter β depends on the evaporation property of the substance, particularly on its latent heat. The value of β is of the order of ten for almost all kinds of liquid at normal temperature. In several cases of sublimation from or condensation on to solid metals, the value of β may become small, or sometimes even negative. Therefore, evaporation or sublimation does not always occur even for smaller value of n_0/n than unity in the case of small β. It should be noted that the vapor may happen to supersaturate in the hydrodynamic region in both cases of evaporation and condensation when β is large as seen from Figs. 8-a, b. Then, some homogeneous re-condensation may occur in the region in practical cases. It seems that such condensation also plays an important role on these phenomena.

Several quasi-steady value of hydrodynamic quantities in the continuum region are plotted as a function of the number flux rate at the interphase, $(nu)_1$, in Figs. 10-a, b, c. Here, all the quantities are presented in such dimensionless forms as $M_\infty=u_\infty/a_\infty$ (local Mach number) and $Q_\infty=q_\infty/(kn_LT_L\sqrt{2RT_L})$ (energy flux), where a_∞ and q_∞ are the isentropic sound speed and the energy flux rate, respectively. Some other theoretical results by Hertz [*1*] and Knudsen [*2*], by Kogan et al. [*10*], by Anisimov [*11*] and by Luikov, et al. [*12*], and a few recalculated values from the experimental data by Golubtsov [*16*] for evaporation of tantalum

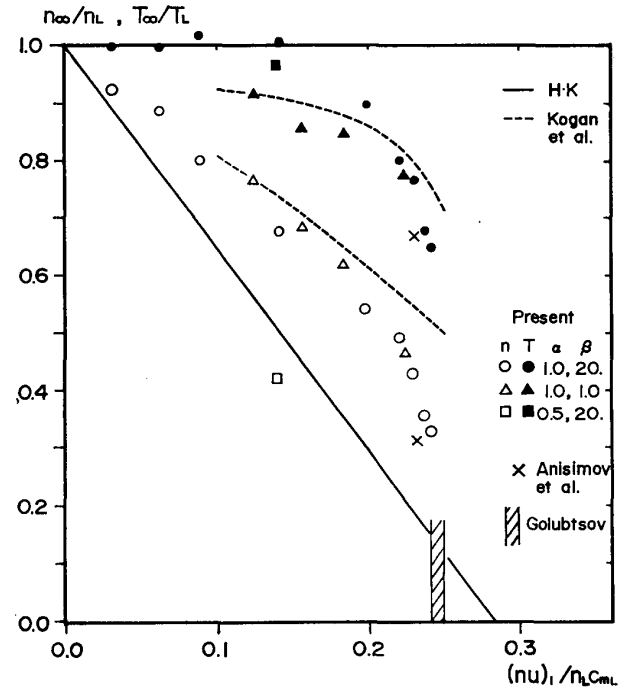

FIG. 10–a. Number density and temperature in hydrodynamic region versus number flux rate for evaporation.

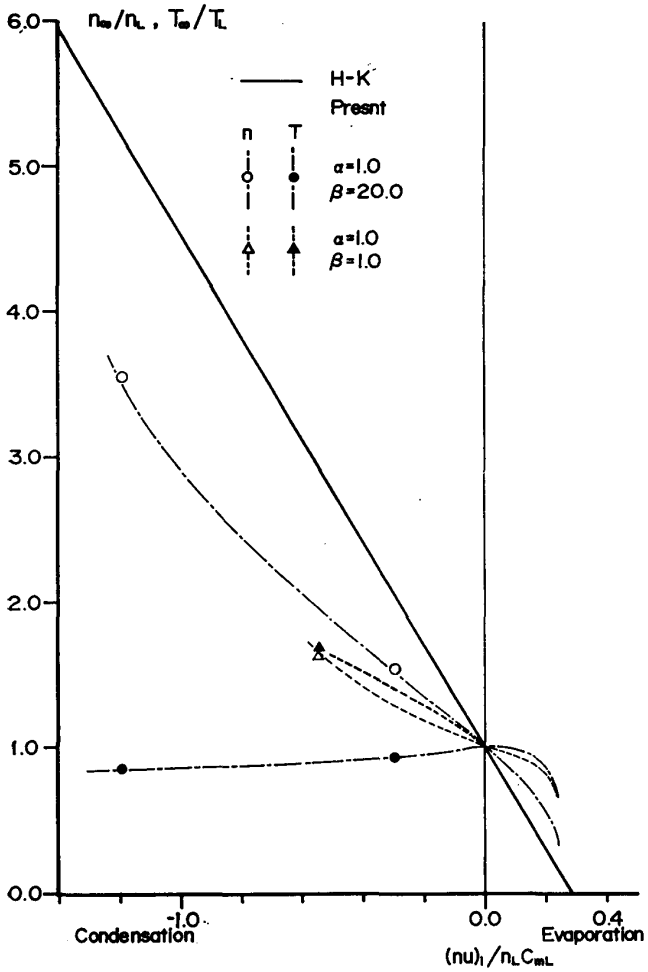

FIG. 10–b. Number density and temperature in hydrodynamic region versus number flux rate for condensation.

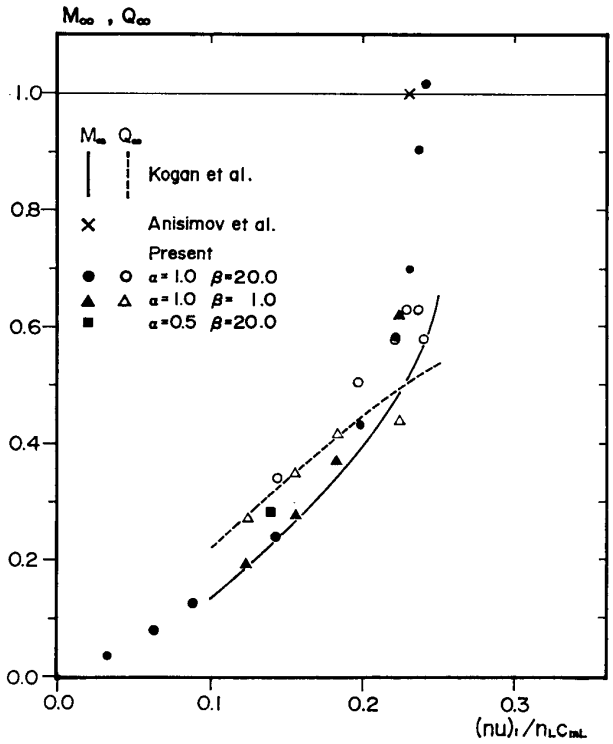

FIG. 10–c. Local Mach number and Heat flux rate in the hydrodynamic region versus number flux rate.

into vacuum are also shown in these figures. The agreement between the two quasi-steady values of the number flux rate evaluated by the use of the equation (34) and by the equation (35) is quite satisfactory, when they are time-averaged over several times of t_0. It is easy to see from the Figs. 10-a, b that the H-K theory considerably underestimates both the evaporation rate and the condensation rate except in the case of very strong evapotation mainly due to disregard of the convective motion of the vapor and of the role of the non-equilibrium Knudsen layer. Here, for the H-K theory one has

$$(nu)_1=(n_L-n_\infty)C_{mL}/2\sqrt{\pi}\,. \tag{36}$$

The agreement of the present results with those by Kogan et al. [*10*] in the case of evaporation is qualitatively satisfactory, especially it is quite good for weak evaporation except the temperature. The relative magnitude of the statistical fluctuation of the present results becomes slightly larger in the case of small $|(nu)_1|$. The results in the case of weak evaporation and comdensation, of course, agree quite well with those predicted using the linear theory presented in several works [*8, 9*]. It is seen from Fig. 10-b that the temperature inversion, that is, the temperature of the vapor, T_∞, becomes lower than T_L in the case of condensation, occurs for $\beta=20.0$ but that no inversion does for $\beta=1.0$. That is because the traveling rarefaction wave due to condensation is dominant and the role of the spontaneously evaporated molecules is relatively weak except in the case of weak, or nearly equilibrium, condensation. It is very important to investigate the be-

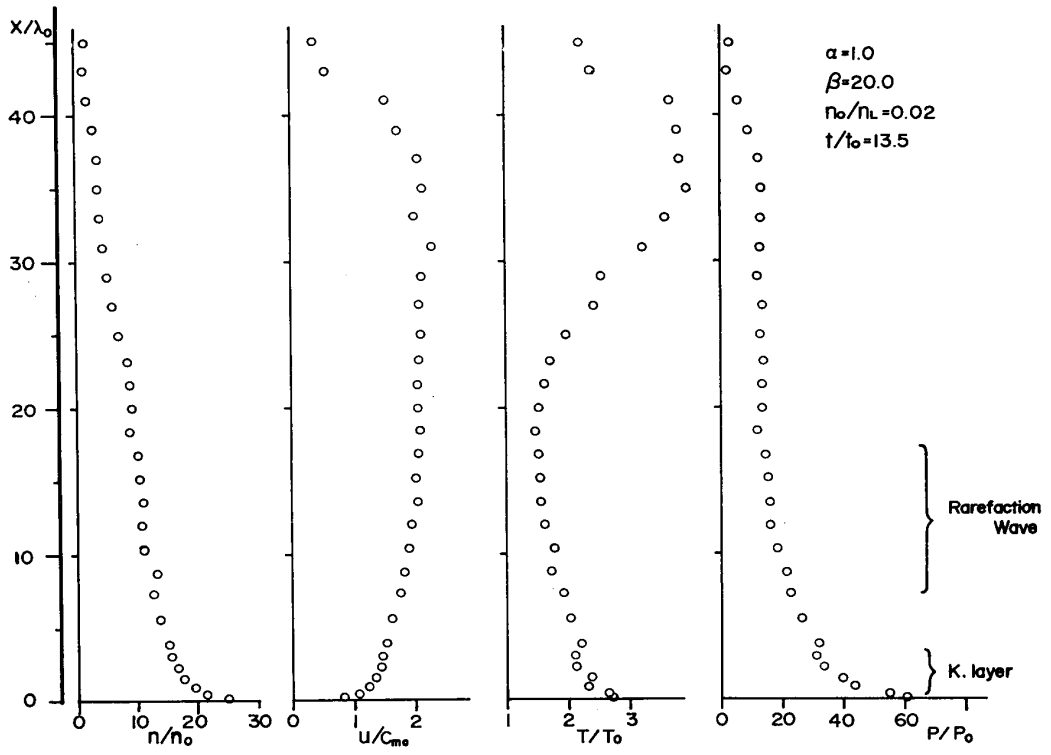

FIG. 11. Vapor profiles in the case with $M_\infty > 1.0$.

havior of strong evaporation. When evaporation becomes stronger, the local Mach number eventually exceeds unity in the hydrodynamic region and the evaporation wave front turns to a shock wave. In such strong evaporation, the vapor is rarefied not only in the Knudsen layer but in the hydrodynamic region and then a cetered rarefaction wave is formed outside the Knudsen layer as seen in Fig. 11. It should be noted that the term of the rarefaction in the Knudsen layer is used in the quite different sense from that in the hydrodynamic region. The state in the layer is far from an equilibrium one, then the rarefaction in the continuum region is not a microscopic but macroscopic, or hydrodynamic in usual sense, phenomenon. It is shown in this figure that the centered rarefaction wave goes after the evaporation wave arising from the outside of the Knudsen layer. Thus, the quasi-steady state is not accomplished any more. Such a state can not be attained also in the case of limiting condensation though the local Mach number never reaches unity, because the tail of the rarefaction wave spreading from the condensation wave front attaches to the outside of the Knudsen layer. It is found from Fig. 10-c that the state computed for $\alpha=1.0$, $\beta=20{,}0$ and $n_0/n_L=0.08$ is in the vicinity of the limiting evaporation, because the Mach number is close to 1.0, and that a quasi-steady state is surely accomplished. It cannot be exactly confirmed owing to the computational fluctuation whether the Mach number surely exceeds unity or not in this case. It follows from Fig. 10-a that the number flux rate has its maximum value. It may be concluded that the maximum value of the number flux rate is reached in the case with the local Mach number of 1.0 and the maximum value is nearly $0.241 \cdot n_L C_{mL}$, which is less than that predicted by

the use of the H-K theory in the steady evaporation. The limiting value of the temperature and the density in the hydrodynamic region are both non-zero. This fact appears to suggest that there is considerable backscattering of the evaporated molecules to the emitting surface as a result of molecular collisions. The quantitative agreement of these results with those by Kogan et al. [*10*] turns gradually poor as evaporation becomes stronger, though their qualitative features are quite similar. In the limit, the present results seem to reach rather close values predicted by using the method proposed by Mott-mith [*11*, *12*], though the present values of the evaporation rate is slightly larger than those by the use of the method. Here, the subscript ∞ for the results by the Mott-Smith method denotes the state at the sonic limit immediately outside the Knudsen layer. Though a quasi-steady state is assumed to be constructed in the continuum region beyond the sonic line in the treatment, it will be, in fact, accomplished asymptotically when $t \to \infty$ because of the propagation of the rarefaction wave from the location of the sonic line. They also agree quite well with the experimental data for tantalum [*16*] as shown in Fig. 10-a. In the case of the limiting evaporation, the Mach number is unity throughout the hydrodynamic region except in the vicinity of the evaporation wave front. The computational results for stronger evaporation than the limit as in Fig. 11 show that the Mach number of the vapor immediately behind the Knudsen layer firstly becomes larger than 1.0 in the initial, or microscopic, stage and then it gradually decreases in the hydrodynamic, or macroscopic, time scale. However, it cannot be confirmed because of the shortage of the computational time whether it falls to unity or not. At any rate, the character of vapor in the neighborhood of the evaporating surface in the case of evaporation into vacuum seems to be approximately described by the use of the Mott-Smith method quite well. That in the full hydrodynamic region could be revealed by the hydrodynamic equations employing the results obtained by the Mott-Smith method as the boundary conditions at the sonic line. That is to say, the flow field consists of the centered rarefaction wave produced immediately behind the Knudsen layer, shock wave at the evaporation front and the uniform region between the two. It is evident in Fig. 10-c that the evaporation rate does not increase in spite of the steep increment of the local Mach number and that the energy flux rate has its maximum value at the limiting situation.

It is also important to note that the effect of β is just a little in the case of evaporation though the transient feature strongly depends on β. On the contrary, the effect is remarkable in the case of condensation. Therefore, such flow parameters as the temperature, the number density, the mass velocity and the energy flux are approximately given as the suitable functions of only the mass flux rate in the case of evaporation but they are mutually related with each other besides the mass flux rate for condensation.

The influence of the mass accommodation coefficient α is large on the number density, because the energy accomodation coefficient is implicitly assumed to be unity. It seems that the influences of such accommodation coefficients are larger

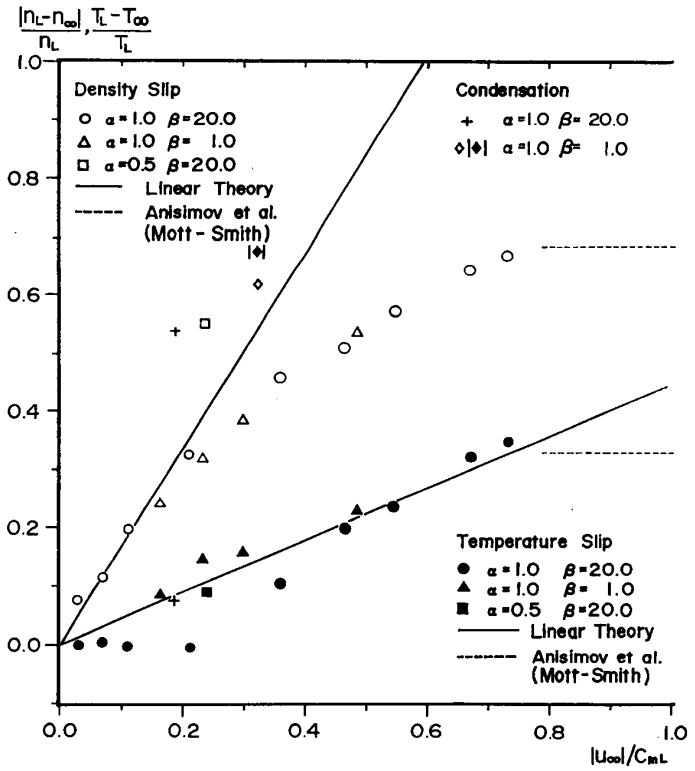

FIG. 12. Number density slip and temperature slip.

on the amounts of the mass and energy transfer rather than on the qualitative feature of these phenomena.

The data presented in Fig. 10-a and 10-b are differently arranged to give the slip condition at the evaporating or condensing surface in hydrodynamic approaches and to compare them with those calculated using the linear theory in Fig. 12. The condition for the extremely strong evaporation obtained by the use of the Mott-Smith method [*11, 12*] is added in this for the sake of comparison. It is an important fact that both slips increase with the mass velocity but are bounded up to the each maximum values less than unity even in the limiting case for evaporation. The agreement of the present results with those estimated using the linear theory is satisfactory in the case of weak evaporation except the temperature for $\beta=20.0$, where the accuracy of the present results does not seem to be sufficient, while rather large discrepancy between the two results is found for the density slip even in the case of the moderately strong evaporation. The limiting values obtained by this simulation agree quite well with those presented in the papers by Anisimov et al. [*11, 12*]. It may be concluded that the slip coefficients derived using the linear theory are valid in the case of weak evaporation for any hydrodynamic approaches. On the other hand in the case of rather strong condensation, the present results are quite different from those by the use of the linear theory as seen from this figure. It is quite natural that the density slip apparently becomes large with the decrease of the value of α.

The evaporation or condensation coefficient f is defined here in the same manner as in the references 14,15 and 18 by

$$f=(nu)_1/(nu)_{1S}, \tag{37}$$

though it has been determined in various procedures, where Schrage's formula $(nu)_{1S}$ is given by

$$(nu)_{1S}=\alpha\left[\Gamma\frac{p_\infty}{(2\pi RT_\infty)^{1/2}}-\frac{p_L}{(2\pi RT_L)^{1/2}}\right]$$
$$\Gamma=\exp(-s^2)-\sqrt{\pi}\,s[1-\mathrm{erf}(s)]$$
$$s=u_\infty/C_{m\infty}.$$

In Fig. 13 the results of the present calculation are shown together with that for the limiting case recalculated from the data appeared in the papers [*11, 12*], which are calculated by the use of the Mott-Smith method. Some scattering of the results in the vicinity of $n_1/n_L=1.0$ is caused by the computational errors due to the statistical fluctuation. This is the reason why two computational values exceed 1.0 in this figure. Though the flow field is not steady for the computational condition of $n_0/n_L=0.02$, a quasi-steady value of the flux rate is obtained. It follows from these data that the coefficient must be close to unity and becomes slightly smaller than 1.0 in the cases of strong evaporation and strong condensation for $\alpha=1.0$. The value obtained using the Mott-Smith method in the case of evaporation into vacuum is 0.836, and the present results seems to approach to the value as the flux rate increases. These conclusions have been also verified experimentally by a few investigators as mentioned before [*14, 15, 16*]. For the ultimately strong evaporation, several values of f have been obtained in the literatures, for example, 0.836 by Anisimov [*11*] and Luikov et al. [*12*], 0.86 from the experimental data by Golubtsov [*16*] and 0.811 by Edwards et al. [*13*]. The parameter β seems to have little effect on this coefficient. It is evident that the absorption coefficient α strongly affects on the value of f but that f is still larger than 0.5 for $\alpha=0.5$. These facts seems to suggest that the kinematic effects of the binary collisions of the vapor molecules that are taken no account of in Schrage's formula are not so

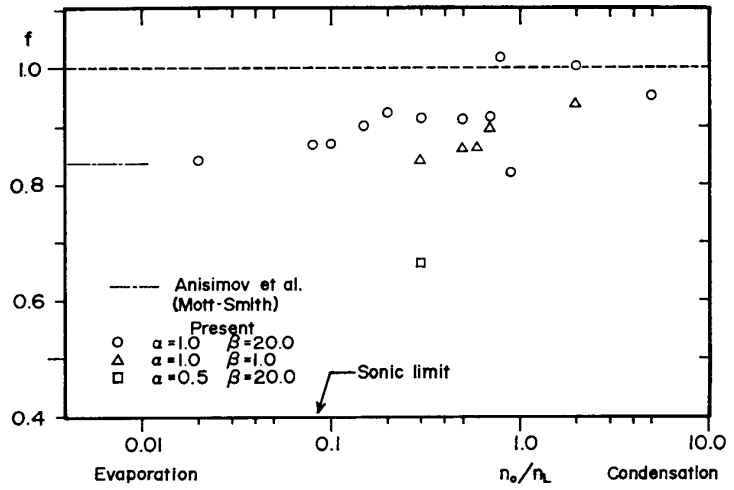

FIG. 13. Evaporation or condensation coefficient.

serious to evaluate the flow rate. However, the vapor field can not be decided without the effects into account.

V. Concluding Remarks

Evaporation and condensation phenomena are investigated with reasonable accuracy by using the Monte Carlo method. It is found that the present results agree quite well with those obtained by the use of the linear theory in the case of weak evaporation and with those estimated using the method proposed by the Mott-Smith in the extremely strong case. The agreement of the data with those by Kogan et al. is qualitatively satisfactorily in all the cases. The H-K theory considerably underestimates the flux rate for both evaporation and condensation. These phenomena are caused by such two transport mechanisms as the wave-like and the diffusion-like ones. Two types of the transient development of the vapor phase seem to be possible of realization, because one of the two mechanisms becomes dominant over the other according to the evaporation property of the condensed phase, say α. The influence of the parameter β on these phenomena is slight for evaporation but is significant for condensation particularly on the temperature of the gas. The evaporation or condensation coefficient seems to be nearly equal to unity and becomes slightly less than 1.0 as the flux rate increases in the case of $\alpha=1.0$. In the case of strong evaporation, the evaporation rate in the steady case is bounded up to almost 24 per cent of $n_L C_{mL}$, of which value is attaianed when the local Mach number throughout the hydrodynamic region becomes unity, since there is considerable backscattering to the phase surface due to molecular collisions. The effects of the binary collisions in the vapor field do not affect seriously the flow rate. It seems that the influences of the accommodation coefficient, say the gas-surface interaction mechanism, dominate over the kinematic effects in the vapor phase on these phenomena.

Department Aerodynamics
Institute of Space and Aeronautical Sciences,
University of Tokyo, Tokyo
October 5, 1974

References

[1] H. Hertz, Ann. Physik, **17** 177 (1882).
[2] M. Knudsen, Ann. Physik, **47**, 697 (1915).
[3] R. W. Schrage, "A Theoretical Study of Interphase Mass Transfer", Columbia Univ. Press, New York (1953).
[4] R. Ya. Kucherov and L. E. Rikenglaz, Soviet Phys. JETP, **37 (10)**, No. 1 (1960).
[5] A. J. Patton and G. S. Springer, in Rarefield Gas Dynamics ed. by H. Trilling and H. Y. Wachman, Vol. II (1969) 1497.
[6] P. N. Shankar and F. E. Marble, Phys. Fluids, **14**, No. 3 (1971) 510.
[7a] Y. P. Pao, Phys. Fluids, **14** (1971) 306.
[7b] Y. P. Pao, Phys. Fluids, **14** (1971) 1340.

[7c] Y. P. Pao, Phys. Fluids, **16** (1973) 1560, also see C. E. Siewert and J. R. Thomas Jr., Phys. Fluids, **16** (1973) 1557.
[*8*] Y. Sone and Y. Onishi, Research Rept. No. 25, Dept. of Aeronautical Engineering, Kyoto Univ. (1973).
[*9*] T. Matsushita, in Rarefied Gas Dynamics XI (1974).
[*10*] M. N. Kogan and N. K. Makashev, Fluid Dynamics, **6**, No. 6 (1974) 913.
[*11*] S. I. Anisimov, Soviet Phys. JETP, **27**, No. 1 (1968) 182.
[*12*] A. V. Luikov, T. L. Perelman and S. I. Anisimov, Int. J. Heat Mass Transfer, **14** (1971) 177.
[*13*] R. H. Edwards and R. L. Collins, in Rarefield Gas Dynamics ed. by H. Trilling and H. Y. Wachman, Vol. II (1969) 1489.
[*14*] N. B. Bakulin, M. N. Ivanovskiy, V. P. Sorokin, V. I. Subbotin and B. A. Chulkov, in MASA TTF-522 (1966) 294.
[*15*] A. F. Mills and A. A. Seban, Int. J. Heat Mass Transfer, **10** (1967) 1815.
[*16*] I. V. Golubtsov, Heat Transfer-Soviet Research, **5**, No. 5 (1973) 18.
[*17*] B. Paul, ARS J. September (1962) 1321.
[*18*] Y. S. Huang, F. A. Lyman and W. J. lick, Int. J. Heat Mass Transfer, **15** (1972) 741.
[*19*] O. F. Hagena and H. von Wedel, in Rarefield Gas Dynamics ed. by M. Becker and M. Fiebig, Vol. II (1974).
[*20*] G. A. Bird, Phys. Fluids, **13**, 11 (1970) 2676.
[*21*] M. Perlmutter, in Rarefield Gas Dynamics ed. by J. H. de Leeuw, Vol. II (1966) pp.-1.
[*22*] J. K. Haviland, in Methods in Computational Physics, **4**, (1065).
[*23*] M. N. Kogan, "Rarefield Das Dynamics", English ed. (1969).